UNIVERSAL WISER
PUBLISHER

Research Article

Numerical Evaluation of the Hydropneumatic Power of the Oscillating Water Column Wave Energy Converter Submitted to Regular and Irregular Waves

Augusto Hack da Silva Koch[1] , **Maycon da Silveira Paiva[2]** , **Caroline Barbosa Monteiro[3]** , **Phelype Haron Oleinik[3]** , **Liércio André Isoldi[3*]** , **Bianca Neves Machado[1,2]**

[1]Federal University of Rio Grande do Sul, Tramandaí, Brazil
[2]Federal University of Rio Grande do Sul, Porto Alegre, Brazil
[3]Federal University of Rio Grande, Rio Grande, Brazil
 Email: liercioisoldi@furg.br

Abstract: The purpose of this study is to computationally analyze the hydropneumatic power available in the air duct of an Oscillating Water Column (OWC) Wave Energy Converter (WEC) device when subject to realistic sea state data (irregular waves) and when submitted to the regular waves representative of this sea state. The OWC WEC is mainly composed of a hydropneumatic chamber and an air duct where a turbine and electric generator are coupled. The chamber is open below the free surface while the duct is open to the atmosphere. The oscillating movement of the water-free surface inside the chamber causes the air to flow, moving the turbine and generating electricity. To execute this study, a bi-dimensional computational model was considered and numerical simulations of wave generation were carried out using ANSYS Fluent, which is a Computational Fluid Dynamics (CFD) software based on the Finite Volume Method (FVM). The Volume of Fluid (VOF) multi-phase model was applied in the treatment of the water-air interaction. To evaluate the average hydropneumatic power available in the duct, the static pressure, velocity, and air mass flow rate were monitored. The results were analyzed, showing that the available power is 250% greater when the device is subject to realistic irregular waves rather than subject to representative regular waves.

Keywords: WaveMIMO methodology, oscillating water column, realistic irregular waves, representative regular waves, computational modeling

1. Introduction

According to Cruz and Sarmento [1], the harnessing wave energy search began in Japan in 1960, with the development of marine signaling buoys powered by wave energy. Mendes [2] states that the ocean waves represent transient mechanical energy resulting from the sum of the kinetic and potential energies of the superficial waves. Through the use of Wave Energy Converter (WEC) devices, such as the Oscillating Water Column (OWC), it is possible to convert the sea wave energy into electrical energy in a renewable way.

As explained by Falcão and Henriques [3], the OWC WEC is essentially composed of a hydropneumatic chamber with a duct where the turbine and the electric generator are coupled. The device has the chamber open under the free

surface of the sea and the duct open to the atmosphere. Thus, the water oscillation inside the chamber, caused by the wave movement, causes local pressure, expelling or suctioning the air through the duct. Finally, the airflow moves the turbine activating the electric generator.

Part of the numerical research carried out in the wave energy area addresses the propagation of regular waves in wave channels reaching WECs, which does not describe the real sea state adequately. More specifically, regarding the regular waves incidence over OWC WECs, one can highlight the following studies: Horko [4] compared the OWC WEC efficiency results obtained from a 2D numerical wave tank model to an experimental model under regular conditions. Elhanafi [5] investigated the hydrodynamic wave loads on an offshore OWC WEC, via a 2D and 3D model, considering different wave climates. Gomes et al. [6] presents a numerical study of the geometry influence on the performance of an OWC WEC through the constructal design method. Conde and Condeço [7], presented the application of the OpenFOAM software package to the numerical simulation of an OWC WEC, comparing the solutions with those obtained by the commercial code ANSYS Fluent. Gaspar et al. [8] compared two geometries for the OWC WEC, concluding that an OWC with inclined walls is more efficient than one with vertical walls.

This simplified approach is valid because it provides relevant recommendations about the operating principle of OWC WEC as well as theoretical recommendations for other studies. However, the results for the available power obtained with this approach do not properly reflect reality since the ocean itself does not have a regular behavior.

Therefore, aiming to obtain a better representation of what occurs in nature, there are studies regarding irregular waves reaching OWC WECs and methodologies for the numerical simulation of irregular waves, such as: Ferguson et al. [9] that compared the operational principle of an OWC WEC subjected to regular, irregular and polychromatic waves using a novel application of normalized histograms. Kim et al. [10] that applied the response spectrum method with the transfer function based on the linear decomposition method to estimate the hydrodynamic energy conversion performance of an OWC device under irregular waves. Machado et al. [11] that developed a methodology that allows the numerical simulation of realistic sea waves and employs it to simulate an OWC device under the sea state of Ingleses Beach, in Florianópolis-SC (Brazil).

Thus, the present study aims to computationally analyze the hydropneumatic power available in the air duct of an OWC WEC when subject to realistic sea state data (irregular waves) and when submitted to the regular waves representative of this sea state. The wave climates were simulated considering a bidimensional numerical wave channel with the OWC device coupled at the end, the average available hydropneumatic power was evaluated in both cases and compared.

For the numerical simulation of realistic sea state, the present paper utilizes the WaveMIMO methodology, as developed by Machado et al. [11]. The data of realistic waves considered in this study reproduces the sea state occurring on March 3, 2018, at 6:45 am at a distance of 171.06 m away from Molhes da Barra, located in Rio Grande City, south region of Rio Grande do Sul state, Brazil. This region was chosen because the Rio Grande has the largest population among the coastal municipalities in the state.

2. Mathematical and computational modeling

For the present study to be performed, numerical simulations of wave generation were carried out using the ANSYS Fluent software, which is a Computational Fluid Dynamics (CFD) software based on the Finite Volume Method (FVM). The multiphase model Volume of Fluid (VOF), proposed by Hirt and Nichols [12] and designated for multiphase flows, was used to treat the interface of the air-water phases, as in Gomes et al. [6], Machado et al. [11] and Lima et al. [13].

For the representation of the phases, it is necessary to understand the volumetric fraction (α) concept, where the sum of the phases in each volume must always be equal to 1. The phases considered in this study are the air and water, thus, the volumes that present values of α_{water} between 0 and 1 contain the interface between water and air, in this case, $\alpha_{air} = 1 - \alpha_{water}$ [14].

A single set of equations is solved in the multiphase VOF model. Thus, the volumetric fraction is considered along with the computational domain through the transport equation. Therefore, according to Versteeg and Malalasekera [15], the model is composed of the continuity equation,

$$\frac{\partial(\rho)}{\partial t} + \nabla \cdot (\rho \vec{v}) = 0 \qquad (1)$$

volumetric fraction transport equation,

$$\frac{\partial(\rho\alpha)}{\partial t} + \nabla \cdot (\rho\alpha\vec{v}) = 0 \qquad (2)$$

and the momentum equation,

$$\frac{\partial}{\partial t}(\rho\vec{v}) + \nabla \cdot (\rho\vec{v}\vec{v}) = -\nabla p + \nabla \cdot (\mu\bar{\bar{\tau}}) + \rho\vec{g} \qquad (3)$$

where ρ is the density of the fluid (kg/m^3), t is the time (s), $\vec{v}$ is the velocity vector (m/s), p is the static pressure (Pa), μ is the dynamic viscosity (kg/ms), $\bar{\bar{\tau}}$ is the stress tensor (Pa) and $\vec{g}$ is the gravity acceleration vector (m/s^2).

2.1 *Wave generation*

The data of realistic waves used in the present paper comes from the TELEMAC-Based Operational Model Addressing Wave Action Computation (TOMAWAC) software [16], which consists of a set of points in space and each point consists of a directional spectrum of waves that varies over time [17]. The representative regular waves, as well as the realistic irregular waves adopted, were generated based on realistic sea state data at the point P (Figure 1) located near the Molhes da Barra in Rio Grande City. Furthermore, Figure 1 represents the computational domain used for the simulation of the sea state on TOMAWAC software.
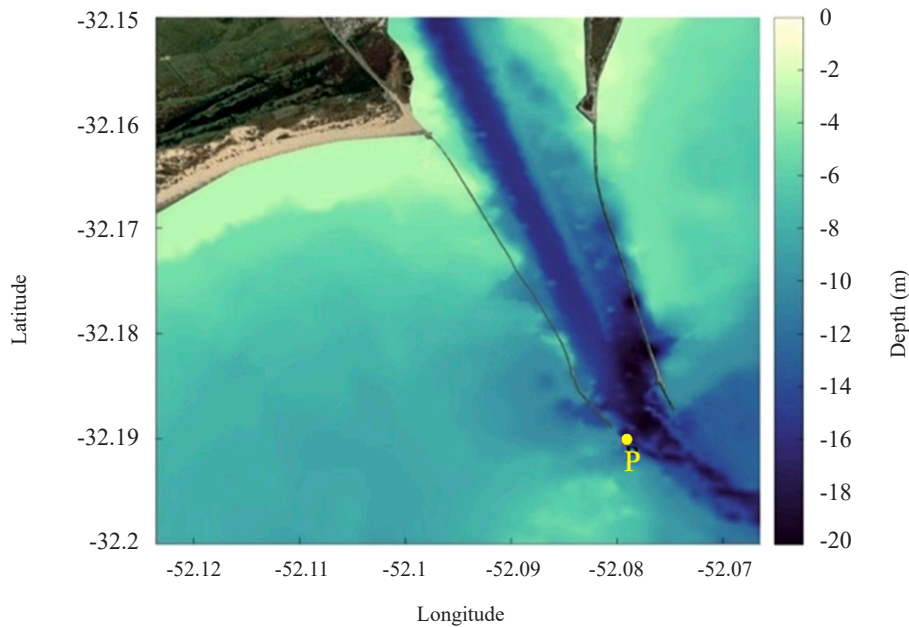

Figure 1. The computational domain used in TOMAWAC for the sea state simulation

As previously stated, the data addressed in this study comes from the spectral model TOMAWAC, they are originated as the solution of Eq. (4), used to conserve the wave action density. This, according to Tavares et al. [18],

represents the general situation of wave propagation in an unsteady and non-homogeneous medium, where the density of wave action (N) is kept within the source term (Q).

$$\frac{\partial N}{\partial t} + \frac{\partial(\dot{x}N)}{\partial x} + \frac{\partial(\dot{z}N)}{\partial z} + \frac{\partial(\dot{k}_x N)}{\partial k_x} + \frac{\partial(\dot{k}_z N)}{\partial k_z} = Q(k_x, k_z, x, z, t) \qquad (4)$$

where N represents the directional spectrum of wave action density (m²/Hz/rad), x the horizontal direction (m), z the vertical direction (m), k_x the component x of the wave number vector, k_z the component z of the wave number vector (1/m), Q is the source term (m²/rad) and t is the time (s).

After the sea state data of the region were obtained, being treated by the Spec2Wave software, which transforms the spectral data generated by TOMAWAC into time series of free surface elevation as well as in horizontal (u) and vertical (w) orbital velocity profiles of wave propagation - more details can be found in Machado et al. [11] and Oleinik [17, 19]. A statistical analysis of the spectral data was performed to estimate the most frequent sea state in the simulated region. Therefore, a bivariate histogram (Figure 2) was elaborated to determine the most frequent combination of significant height (H_s) and the mean period (T_m) of the waves.
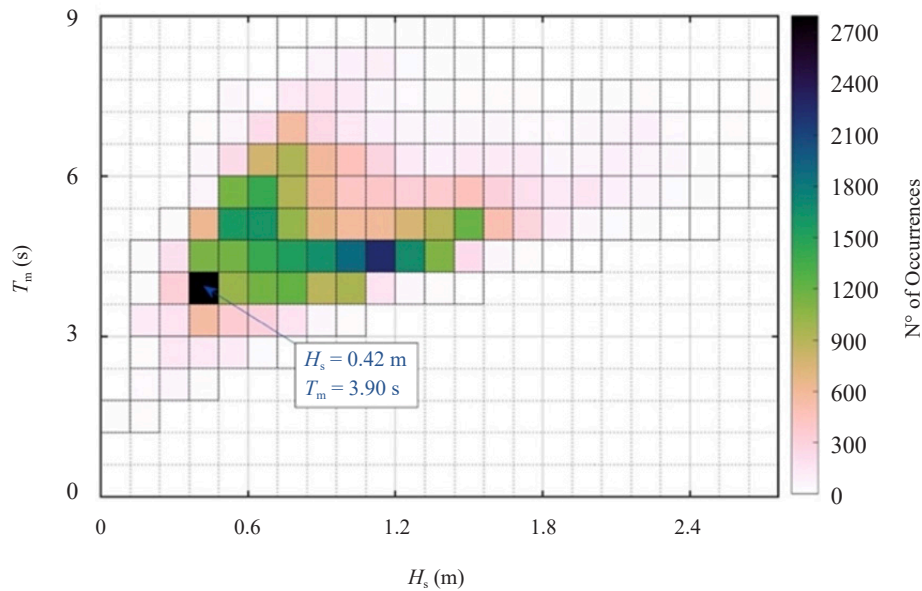

Figure 2. Histogram of wave recurrence relating T_m and H_s

Observing Figure 2, it is possible to conclude that the most frequent sea state in the region during the evaluated time interval is represented by the combination of $H_s = 0.42$ m and $T_m = 3.90$ s. Thus, these data were adopted as characteristics for the representative regular waves. The wavelength (λ) can be obtained by solving k for the dispersion relation [20]:

$$\omega^2 = g\,k\,tanh(kh) \qquad (5)$$

where the angular wave frequency ω is related to wave period T (s) by $\omega = 2\pi/T$, the angular wave number k is related to wavelength λ by $k = 2\pi/\lambda$, and g is the acceleration of gravity. The characteristics of the representative regular waves performed in the study can be observed in Table 1.

Table 1. Characteristics of the sea state representative regular waves

Characteristic	Nomenclature	Value
Wave period	T (s)	3.90
Wave height	H (m)	0.42
Wavelength	λ (m)	23.69
Water depth	h (m)	13.29

For the representative regular waves generation, the horizontal (u) and vertical (w) prescribed velocity boundary conditions are imposed on the entrance side of the wave channel. According to McCormick [21] and Dean and Dalrymple [20], the velocities are given, respectively, by:

$$u = \frac{H}{2} gk \frac{\cosh(kz + kh)}{\omega \cosh(kh)} \cos(kx - \omega t)$$

(6)

$$w = \frac{H}{2} gk \frac{\sinh(kz + kh)}{\omega \cosh(kh)} \sin(kx - \omega t)$$

(7)

where $H/2$ is the wave amplitude (m).

Furthermore, the water free surface elevation can be described analytically for regular waves, such as [20]:

$$\eta = \frac{H}{2} \cos(kx - \omega t)$$

(8)

where η is the free surface elevation (m).

Finally, following the WaveMIMO methodology [11], the generation of realistic waves in the ANSYS Fluent software occurs through the imposition of discretized orbital velocity profiles, horizontal (u) and vertical (w), as boundary conditions. Therefore, the methodology requires the discretization of the inlet region of the channel, where these prescribed velocities are imposed (red line of Figure (3a)). Thus, this region was divided into 21 sub-regions (yellow and black dashed line in Figure 3(b)), enabling the imposition of data as boundary conditions. It is worth mentioning that the imposition of discrete data of the velocities u and w to generate regular waves was already validated in Maciel et al. [22].
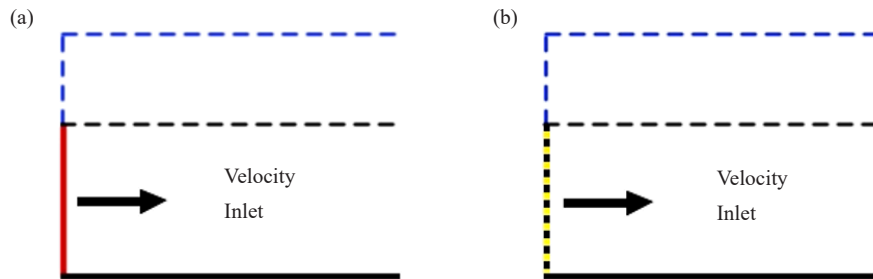

Figure 3. Illustration of the imposition region of velocity inlet boundary condition: (a) for the representative regular waves; (b) for the realistic irregular waves

2.2 Computational domain

As already mentioned, the present study aims to evaluate the hydropneumatic power available on the air duct of the OWC device when submitted to regular and irregular waves. The computational model for the regular waves is based on [23], while the irregular waves were generated by the computational model based on Machado et al. [11] and Maciel et al. [22].

The WEC devices can be classified according to the depth of installation onshore (coastal devices that are accessible through the land); nearshore (devices near the coast); and offshore (devices away from the coast) [1]. According to this classification, the device approached in the study consists of an onshore WEC, thus, it was considered a bidimensional computational domain composed of a wave channel with the OWC device coupled in its end.

The wave channel used in the study has a length $L = 171.06$ m and reproduces, on its bottom, the bathymetry found in the Molhes da Barra region, where the sea state data were simulated. Thus, the depth of the channel varies from $h_1 = 13.29$ m, in the wave generation zone, to $h_2 = 10.54$ m, in the OWC zone, representing the region near the coast. The illustration of the computational domain is displayed in Figure 4.
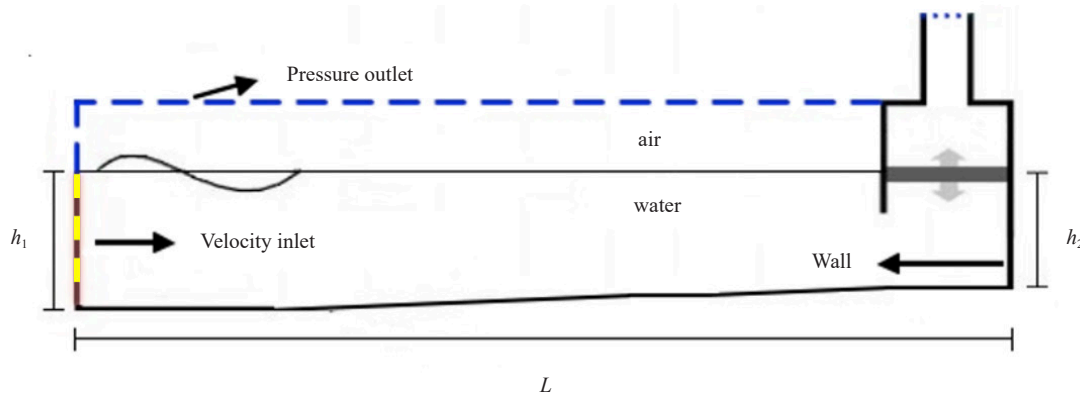

Figure 4. Representation of the computational domain adopted

As for the boundary conditions, they are prescribed velocity (velocity inlet), in the wave generation region (black and yellow dashed line in Figure 4), as previously indicated (see Figure 3(b)); atmospheric pressure, in the upper left segment and at the top of the wave channel, in addition to the duct outlet (blue dashed line in Figure 4); wall (nonslip and impermeability), at the bottom of the channel and in the OWC device (black continuous line in Figure 4). It is worth noting that the boundary conditions, the characteristics of the wave channel, and the OWC WEC were kept identical for both simulated cases.

The characteristics of the OWC WEC adopted in this study are the same characteristics adopted by Gomes et al. [23]. The dimensions of the simulated OWC WEC are illustrated in Figure 5.

Regarding the spatial discretization of the computational domain, a stretched mesh was used, as recommended by Gomes et al. [24]. This mesh is characterized for applying better refinement in the water-free surface region. Then, considering Figure 6, the computational domain was divided into three vertical regions: R1, the region above the free surface, which contains only air, subdivided into 20 elements; R2 in the free surface region, where water-air interaction occurs, subdivided into 40 elements; and R3, region below the free surface, containing only water, subdivided into 60 elements. Horizontally, the computational domain was divided into two regions: R4, the region before the OWC WEC discretized into 50 elements per wavelength; R5 region referring to the interior of the device, discretized in quadrilaterals of side $\Delta x = 0.01$ m, as recommended by Lima et al. [13]. Finally, regarding temporal discretization, 100 s were simulated using $\Delta t = T/500$ as the time step, as indicated by Gomes et al. [25].
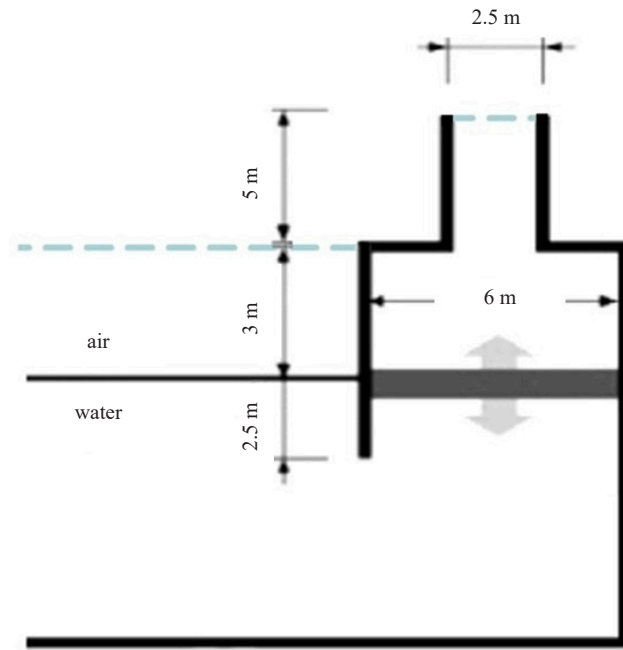
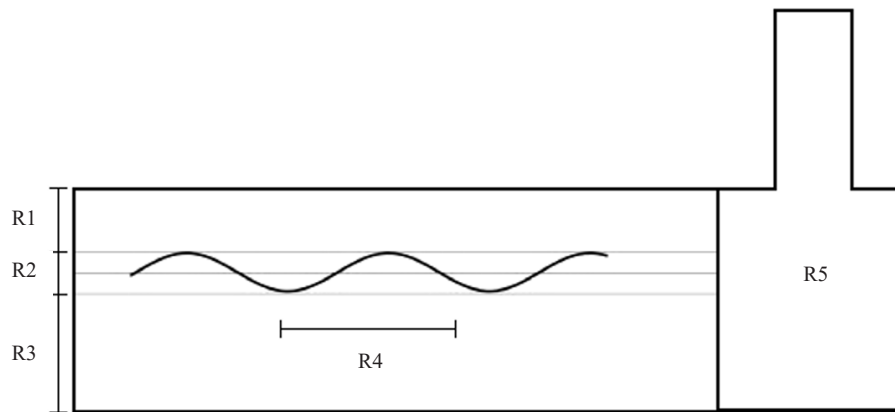**Figure 5.** Characteristics of the OWC WEC (adapted from Gomes et al. [23])

Figure 6. Illustration of the regions used in the stretched mesh

As previously mentioned, the present study uses two different forms to represent the sea state in the studied interval time and place: the realistic irregular waves and the representative regular waves. Therefore, it is worth highlighting that to carry out the necessary discretization for the stretched mesh, the wave period and wavelength of the representative regular waves were considered in both cases.

To monitor the free surface elevation, a vertical probe of the integral type was used in the position $x = 0$ m, i.e, in the region of imposition of the velocity inlet boundary condition, since the realistic data from TOMAWAC refer to this point. To evaluate the average hydropneumatic power, a horizontal probe was used in the center of the duct of the OWC device aiming to monitor the static pressure, air velocity, and air mass flow rate in that region.

3. Results

To verify the employed methodology, the water free surface elevation data monitored by the probe were used. While for the case of the regular wave, the evaluation was carried out comparing the data obtained in the present study with the analytical solution for surface elevation given through Eq. (8); for the realistic irregular waves case, the monitored data were compared to the realistic sea state data obtained on the TOMAWAC software. The mentioned comparison is displayed in Figure 7(a) the representative regular waves and in Figure 7(b) the realistic irregular waves.
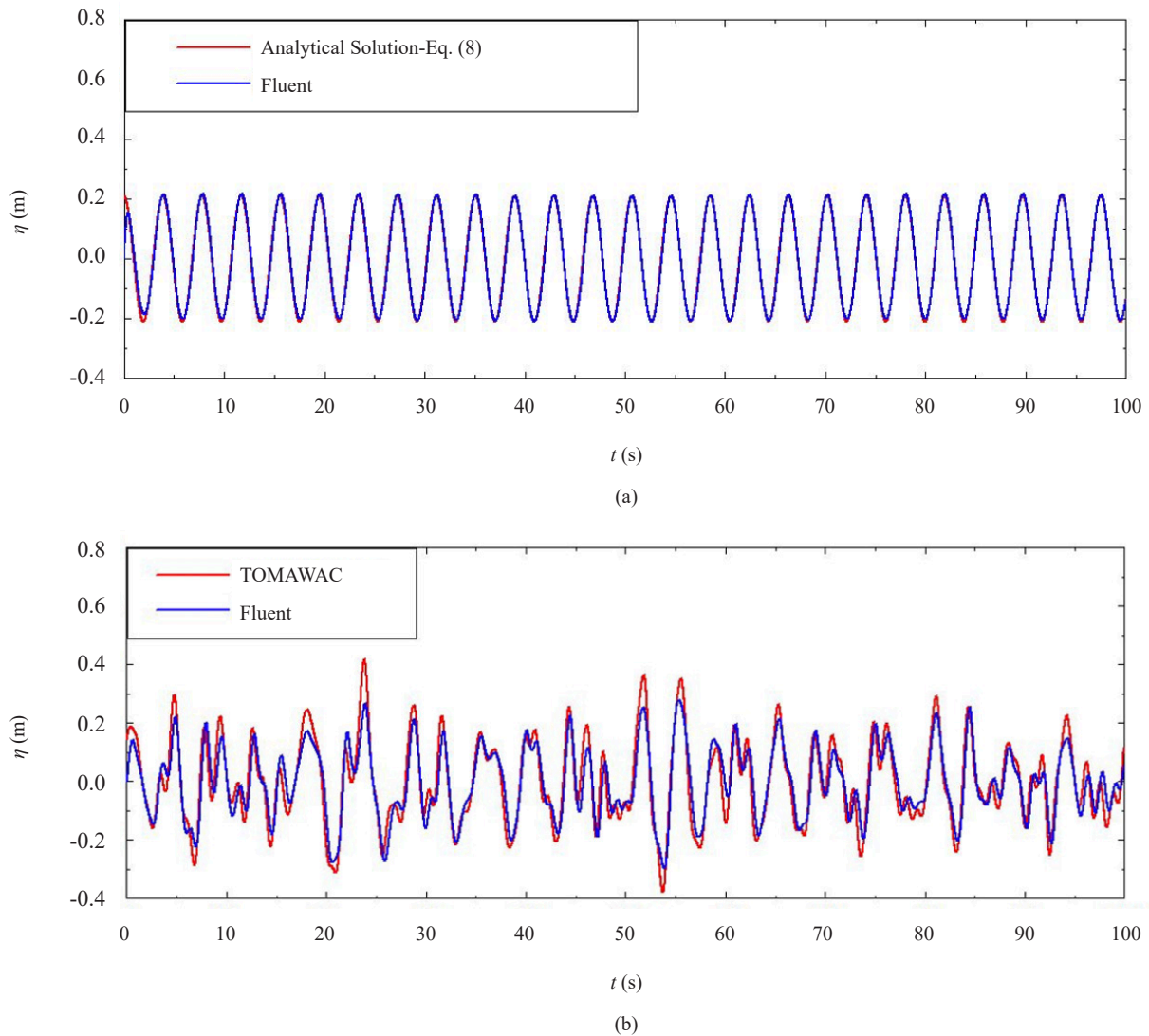

(a)

(b)

Figure 7. Comparison between the free surface elevation on (a) representative regular waves generation; (b) realistic irregular waves generation

On the other hand, a more accurate alternative for analyzing the results is performed through the evaluation of numerical error. Thus, the results were analyzed through the calculation of error metrics Mean Absolute Error (MAE) and Root Mean Square Error (RMSE), defined, respectively, as [26]:

$$MAE = \sum_{i=1}^{n} \left| \frac{R_i - E_i}{n} \right| \tag{9}$$

$$RMSE = \sqrt{\frac{\sum_{i=1}^{n}(R_i - E_i)^2}{n}} \tag{10}$$

where R_i represents the reference values defined by the analytical solution (representative regular waves case) or the data obtained through the TOMAWAC software (realistic irregular waves case), E_i represents the values found numerically and n is the number of points in the dataset.

Results obtained are presented in Table 2, verifying the computational model used.

Table 2. Results of MAE and RMSE

Waves	MAE (m)	RMSE (m)
Representative Regular	0.007	0.008
Realistic Irregular	0.042	0.052

To compare the theoretical power available in the OWC duct for each of the waves, the available instantaneous hydropneumatic power was calculated, as indicated in Gomes et al. [6], by:

$$P_H = \left(p + \frac{\rho v^2}{2} \right) \frac{\dot{m}}{\rho} \tag{11}$$

where P_H is the available instantaneous hydropneumatic power (W), p is the static pressure (Pa), $\dot{m}$ is the mass flow rate of air (kg/s) and v is the air velocity in the vertical direction (m/s) inside the duct.
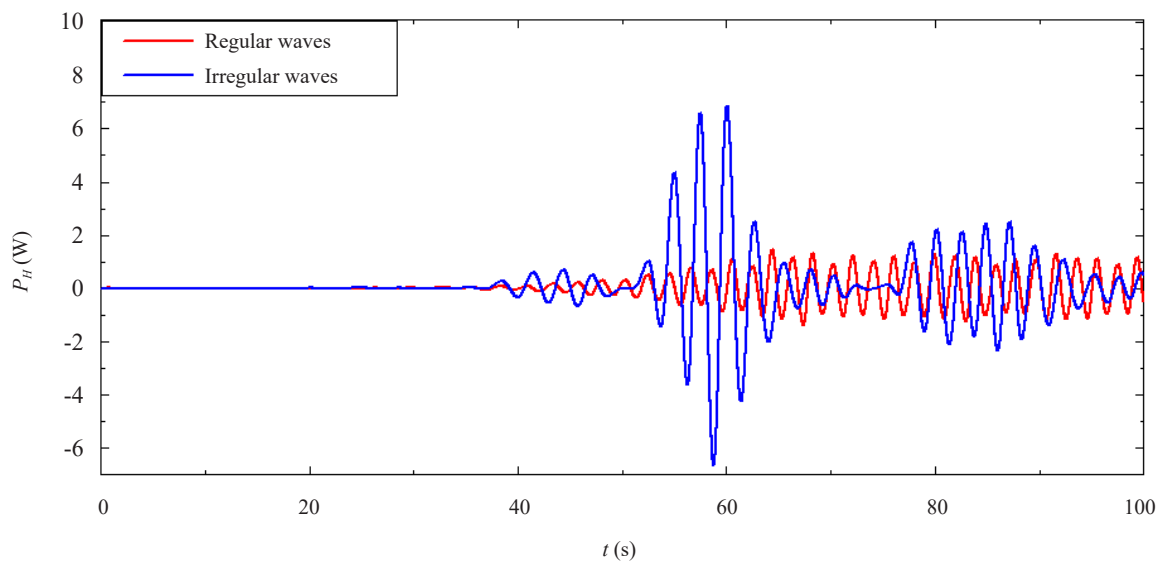

Figure 8. Results for the instantaneous hydropneumatic available power in the OWC WEC

Figure 8 shows the available hydropneumatic power obtained over the 100 s of simulation for the two approaches considered in this study. Qualitatively, as expected, it is observed that the power obtained from the realistic irregular waves presents greater oscillation, while the power extracted from the regular waves has greater stability from $t \approx 40$ s instant when the wave hits the OWC device in both cases. It is also observed that the instantaneous hydropneumatic available power reaches maximum values in the interval 55 s $\leq t \leq$ 65 s.

To determine the available hydropneumatic power value for each case during the time interval considered, the Root Mean Square (RMS) average of the P_H was calculated, in accordance with [27]:

$$P_{RMS} = \sqrt{\frac{\sum_{i=1}^{n}(P_{H(i)})^2}{n}} \tag{12}$$

where P_{RMS} represents the calculated RMS average for the P_H. Table 3 shows the available average hydropneumatic power (P_{RMS}) in each case.

Table 3. Available average hydropneumatic power

Waves	P_{RMS} (W)
Representative Regular	0.515
Realistic Irregular	1.292

Analyzing Table 3, it is possible to infer that the available hydropneumatic power during the simulation of realistic irregular waves is around 2.5 times greater than that generated during the simulation of representative regular waves. It is believed that the biggest instantaneous hydropneumatic available power occurred when the OWC WEC was subjected to the realistic irregular waves due to the fact these waves present in a general way crests and troughs larger than crests and troughs of the representative regular waves (see Figure 7). Hence, these larger crests and troughs generate a larger mass flow rate of air in the OWC duct during the simulated interval time, which according to Eq. (11), promotes a larger instantaneous available hydropneumatic power. Thereby, this study shows the importance of using the irregular waves approach, generated from a realistic sea state, when numerically evaluating the theoretical potential of an OWC WEC.

4. Conclusion

The present study shows the comparison between numerical simulations considering regular and irregular waves on the coast of the city of Rio Grande in southern Brazil, using as base a sea state of significant height (H_s) and the mean period (T_m) corresponding to the most frequent sea state at the studied region in 2018. The selected sea state was used to generate transient profiles of wave orbital velocities, which were then imposed as boundary conditions of prescribed velocity in the ANSYS Fluent software when simulating irregular waves, following the WaveMIMO methodology. Aiming to compare the OWC WEC functionality, representative regular waves were also simulated with height H equal to H_s and period T equal to T_m.

The results showed that the simulations performed reproduced adequately the waves imposed on the model, with an RMSE of approximately 0.05 m for realistic irregular waves and approximately 0.01 m for representative regular waves, when comparing the ANSYS Fluent results respectively to the original elevation time series of TOMAWAC and the analytical solution given by Eq. (8).

In addition, the average available hydropneumatic power in the simulated OWC device was calculated for each case. The results showed that realistic irregular waves generated an available average power around 2.5 times greater than the available average power provided by representative regular waves.

The results of the present work indicated that the use of H_s and T_m as the only predictors of the sea state, such as in the case of regular waves, might lead to inaccurate results when simulating the WECs. In this case, the available average power in the OWC device was reduced by approximately 60% when subjected to the incidence of representative regular waves, emphasizing the importance of using realistic sea state data for the WEC studies since irregular waves better represent the sea state, which is also irregular.

The differential of this study is the usage of the WaveMIMO methodology for irregular waves generation. For future studies is aimed to keep using this methodology to the simulation of longer interval time for the propagation of the irregular waves; as well as to the simulation of different geometries for the WECs submitted to this sea state. In addition, enabling through the Constructal Design and exhaustive search for geometrical optimization of an OWC WEC device to the Molhes da Barra in Rio Grande City.

Acknowledgements

Conflict of interest

The authors declare no conflict of interest.

References

[1] J. M. B. P. Cruz and A. J. N. A. Sarmento, *Wave Energy: Introduction to Technological, Economic and Environmental Aspects*. Institute of the Environment, 2004.

[2] R. P. G. Mendes, "Wave energy: development of a generation technology: tubular generator," M. S. thesis, University of Beira Interior, Covilhã, Portugal, 2011.

[3] A. F. O. Falcão and J. C. C. Henriques, "Oscillating-water-column wave energy converters and air turbines: A review," *Renewable Energy*, vol. 85, pp. 1391-1424, 2016.

[4] M. Horko, "CFD optimisation of an oscillating water column wave energy converter," M. S. thesis, University of Western, Australia, 2007.

[5] A. Elhanafi, "Prediction of regular wave loads on a fixed offshore oscillating water column-wave energy converter using CFD," *Journal of Ocean Engineering and Science*, vol. 1, no. 4, pp. 268-283, 2016.

[6] M. N. Gomes, G. Lorenzini, L. A. O. Rocha, E. D. Dos Santos, and L. A. Isoldi, "Constructal design applied to the geometric evaluation of an oscillating water column wave energy converter considering different real scale wave periods," *Journal of Engineering Thermophysics*, vol. 27, pp. 173-190, 2018.

[7] J. Conde and M. Condeço, "Numerical simulation of an Oscillating Water Column (OWC) Wave Energy Converter (WEC) on a breakwater using OpenFOAM," *Defect and Diffusion Forum*, vol. 396, pp. 12-21, 2019.

[8] L. A. Gaspar, P. R. Teixeira, and E. Didier, "Numerical analysis of the performance of two onshore oscillating water column wave energy converters at different chamber wall slopes," *Ocean Engineering*, vol. 201, pp. 107-119, 2020.

[9] T. M. Ferguson, I. Penesis, G. Macfarlane, and A. Fleming, "A PIV investigation of OWC operation in regular, polychromatic and irregular waves," *Renewable Energy*, vol. 103, pp. 143-155, 2017.

[10] J. S. Kim, K. H. Kim, J. Park, S. Park, and S. H. Shin, "A numerical study on hydrodynamic energy conversions of OWC-WEC with the linear decomposition method under irregular waves," *Energies*, vol. 14, no. 6, 2021.

[11] B. N. Machado, P. H. Oleinik, E. Kirinus, E. D. Dos Santos, L. A. O. Rocha, M. N. Gomes, J. P. Conde, and L. A. Isoldi, "WaveMIMO methodology: numerical wave generation of a realistic sea state," *Journal of Applied and*

Computational Mechanics, vol. 1, pp. 1-20, 2021.

[12] C. W. Hirt and B. D. Nichols, "Volume of Fluid (VOF) method for the dynamics of free boundaries," *Journal of Computational Physics*, vol. 39, pp. 201-225, 1981.

[13] Y. T. B. Lima, M. N. Gomes, C. F. Cardozo, L. A. Isoldi, E. D. Dos Santos, and L. A. O. Rocha, "Analysis of geometric variation of three degrees of freedom through the constructal design method for a oscillating water column device with double hidropneumatic chamber," *Defect and Diffusion Forum*, vol. 396, pp. 22-31, 2019.

[14] L. Ling, C. Yongcan, and L. Yuliang, "Volume of Fluid (VOF) method for curved free surface water flow in shallow open channel," Department of Hydraulic Engineering, Tsinghua University, Beijing, China, 2001.

[15] H. K. Versteeg and W. Malalasekera, *An Introduction to Computational Fluid Dynamics: The Finite Volume Method*. Prentice-Hall, 2007.

[16] T. Awk, *TOMAWAC User Manual*, version 7.2, 7.2.3 ed., The TELEMAC-Mascaret Consortium, 2017.

[17] P. H. Oleinik, *The Spec2Wave software: User Manual*. 2019.

[18] G. P. Tavares, R. P. Maciel, E. D. Dos Santos, M. N. Gomes, L. A. O. Rocha, B. N. Machado, P. H. Oleinik, and L. A. Isoldi, "A comparative numerical analysis of the available power between regular and irregular waves: Case study of an oscillating water column converter in Rio Grande Coast," presented at 18th Brazilian Congress of Thermal Sciences and Engineering (ENCIT), Rio de Janeiro, Brazil, 2020.

[19] P. H. Oleinik, "Numerical methodology for the hydrodynamic simulation of sea states using spectral wave data and case study of an owc on the coast of Rio Grande-RS," M. S. thesis (in Portuguese), Federal University of Rio Grande, RG, 2020.

[20] R. G. Dean and R. A. Dalrymple, *Water Wave Mechanics for Engineers and Scientists*. World Scientific, Singapura, 1991.

[21] M. E. McCormick, *Ocean Engineering Mechanics. New York.* Cambridge University Press, 1976.

[22] R. P. Maciel, C. Fragassa, B. N. Machado, L. A. O. Rocha, E. D. Santos, M. N. Gomes, and L. A. Isoldi, "Verification and validation of a methodology to numerically generate waves using transient discrete data as prescribed velocity boundary condition," *Journal of Marine Science and Engineering*, vol. 9, no. 896, pp. 1-19, 2021.

[23] M. N. Gomes, L. A. Isoldi, C. R. Olinto, L. A. O. Rocha, E. D. Dos Santos, and J. A. Souza, "Computational modeling of an oscillating water column device for the Rio Grande Coast," *Vetor*, vol. 19, no. 2, pp. 58-73, 2009.

[24] M. N. Gomes, L. A. Isoldi, E. D. Dos Santos, and L. A. O. Rocha, "Analysis of Meshes for Numerical Wave Generation in Tanks," presented at VII Congresso Nacional de Engenharia Mecânica (CONEM), São Luís, Maranhão, Brasil, 2012.

[25] M. N. Gomes, L. A. Isoldi, E. D. Dos Santos, and L. A. O. Rocha, "Numerical simulation of regular wave propagation in Tanks," in *Wave Propagation*, L. A. O. Rocha and M. N. Gomes, Eds. Cheyenne: Academicpublish. Org (Publishing Services), 2014, pp. 115-134.

[26] T. Chai and R. R. Draxler, "Root Mean Square Error (RMSE) or Mean Absolute Error (MAE)?-Arguments against avoiding RMSE in the literature," *Geoscientific Model Development*, vol. 7, no. 3, pp. 1247-1250, 2014.

[27] L. H. Holthuijsen, *Waves in Oceanic and Coastal Waters*. Cambridge: Cambridge University Press, 2007.